
Article:
Ziegler, K, Tumova, S, Kerimi, A et al. (1 more author) (2015) Cellular asymmetric catalysis by UDP-glucuronosyltransferase 1A8 shows functional localization to the basolateral plasma membrane. Journal of Biological Chemistry. ISSN 1083-351X

https://doi.org/10.1074/jbc.m114.634428

Cellular Asymmetric Catalysis by UDP-glucuronosyltransferase 1A8 Shows Functional Localization to the Basolateral Plasma Membrane

Kerstin Ziegler [1], Sarka Tumova [1], Asimina Kerimi [1] and Gary Williamson [1]

[1]Faculty of Mathematics and Physical Sciences,
University of Leeds, Leeds, LS2 9JT, UK

To whom the correspondence should be addressed: Gary Williamson, University of Leeds, Leeds, LS2 9JT, UK, G.Williamson@leeds.ac.uk, Tel.: +44 0113 343 8380, Fax: +44 113 343 2982

*Running Title: Asymmetric UGT1A8 activity

Keywords: cell polarity, membrane enzyme, polyunsaturated fatty acid, xenobiotics, intestinal metabolism, flavonoid, UDP-glucuronosyltransferase, fatty acid

Background: Conjugating enzymes such as UDP-glucuronosyltransferases (UGTs) determine small molecule bioavailability.
Results: UGT1A8 is induced by certain fatty acids and functionally localizes in the basolateral plasmalemma in HT29-MTX goblet cells.
Conclusion: The conjugation pattern is asymmetric, suggesting association of UGT1A8 with membrane transporters.
Significance: The enzyme localization allows the cell to carry out conjugation without the small molecule entering into the interior of the cell.

Abstract

UDP-glucuronosyltransferases (UGTs) are highly expressed in liver, intestine and kidney and catalyze the glucuronic acid conjugation of both endogenous compounds and xenobiotics. Using recombinant human UGT isoforms, we show that glucuronic acid conjugation of the model substrate, (-)-epicatechin, is catalyzed mainly by UGT1A8 and UGT1A9. In HepG2 cells, pre-treatment with polyunsaturated fatty acids increased substrate glucuronidation. In the intestinal Caco-2/HT29-MTX co-culture model, overall relative glucuronidation rates were much higher than in HepG2 cells and (-)-epicatechin was much more readily conjugated when applied to the basolateral side of the cell monolayer. Under these conditions, 95% of the conjugated product was effluxed back to the site of application and none of the other phase 2-derived metabolites followed this distribution pattern. HT29-MTX cells contained >1000-fold higher levels of UGT1A8 mRNA than Caco-2 or HepG2 cells. Gene expression of UGT1A8 increased after treatment of cells with docosahexaenoic acid, as did UGT1A protein levels. Immunofluorescence staining and western blotting showed the presence of UGT1A in basal and lateral parts of the plasma membrane of HT29-MTX cells. These results suggest that in HT29-MTX goblet cells at least some of the UGT1A8 enzyme is not endoplasmic reticulum resident but plasma membrane spanning, resulting in much more efficient conjugation of substrate from the basal than from the luminal side, coupled with rapid efflux by functionally-associated basolateral transporters. This novel molecular strategy allows the cell to carry out conjugation without the xenobiotic entering into the interior of the cell.

The group of UDP-glucuronosyltransferase (UGT) enzymes are a large family involved in phase II metabolism. In vertebrates, the UGT protein spans the endoplasmic reticulum (ER) membrane with the active site facing the ER lumen (1). UGTs

catalyze the transfer of glucuronic acid from the co-factor UDP-glucuronic acid (UDPGA) to a nucleophilic group of the substrate, increasing the size and polarity of the compound and thus enabling active transport and cellular efflux (2). UGTs display broad substrate specificity ranging from drugs (3,4) to environmental pollutants (5-7) and endogenous compounds (8-11). Polyphenols such as (-)-epicatechin, plant derived phenolic substances which inhibit NADPH-oxidase, affect NO signalling and modulate endothelial function (for a recent review, see (12)), are very efficiently conjugated with glucuronic acid (13-15). Glucuronidation dramatically affects the distribution and biological activity of (-)-epicatechin as well as endogenous compounds such as bile acids (13,16-18). Phase II metabolism is almost entirely facilitated by the UGT1A and UGT2B families (19), with the highest UGT activity found in liver and intestine. Ohno and Nakajin analyzed samples from various tissues for relative mRNA abundance of different UGT isoforms. Overall, they reported much higher levels of UGT2B than UGT1A forms, except for UGT1A9 which is highly expressed in kidney. The main UGT2B isoforms in hepatic tissue are UGT2B4 and UGT2B15, and the main UGT1A forms are UGT1A1 and UGT1A9. In the intestine, UGT2B7, UGT2B17, UGT1A1 and UGT1A10 were most abundant (20).

The impact of dietary fatty acids on UGT activity has been investigated with inconsistent results. Some studies found that fatty acids could inhibit UGT activity, whereas others concluded that they increase conjugation rates. (21-27).

Upon entering the cell, fatty acids are bound by fatty acid binding protein (FABP) and then either esterified and stored as triglycerides or coenzyme A conjugated and used for energy production (28). The effect of acyl-CoAs on UGT activity in vitro depends on concentration and microsomal pre-treatment with de-latency agents (e.g. detergents or alamethicin). High acyl-CoA concentrations inhibited, but lower concentrations enhanced UGT activity. In intact microsomes, acyl-CoAs and free unsaturated fatty acids resulted in activity enhancement, but in detergent-treated microsomes activity was reduced (29). Unsaturated fatty acids could inhibit glucuronidation of 4-methyl-umbelliferone by human kidney cortical microsomes and recombinant UGT1A9 and UGT2B7 enzymes. The greater the degree of fatty acid unsaturation, the more pronounced the inhibition (30).

Studies using recombinant enzyme found that PUFAs inhibited UGT1A1 glucuronidation of estradiol in vitro with docosahexaenoic acid (DHA) having the greatest effect. DHA also inhibited enzyme activity in vivo, increasing bilirubin levels 48 h after oral administration of low concentrations of DHA, but high DHA concentrations had the opposite effect. (31). In addition, this and other studies have reported an increase in UGT expression with unsaturated fatty acid feeding. This could be explained by in vitro results which show that PUFA metabolites of the lipoxygenase or cyclooxygenase pathways and some free fatty acids activate peroxisome proliferator-activated receptors α and γ (PPARα, PPARγ) which then stimulate UGT gene transcription (32-34).

The examples given above indicate that fatty acids can have a different impact on UGT activity and expression depending on the model and conditions employed. In the present study, different tissue culture models were employed to investigate the effect of dietary fatty acids on glucuronidation of (-)-epicatechin. This compound was chosen as there are increasing numbers of reports on the effects of this class of compounds on NO metabolism, and glucuronidation of (-)-epicatechin has so far not been observed in vitro (35) despite evidence that (-)-epicatechin is extensively conjugated with glucuronic acid in vivo (36,37).

EXPERIMENTAL PROCEDURES

Chemicals, cell lines and reagents

All cell culture consumables, acetonitrile, formic acid, stearic, linolenic and arachidonic acid, (-)-epicatechin, 3,4-dimethoxycinnamic acid, ascorbic acid and protease inhibitor cocktail were purchased from Sigma-Aldrich (St. Louis, USA), RIPA buffer, EZ-Link Sulfo-NHS-LC-Biotin, High Capacity Streptavidin Agarose Resin and bicinchoninic acid (BCA) kit were purchased from Pierce Biotechnology (Rockford, USA), eicosapentaenoic acid (EPA) and DHA were purchased from Cayman Chemical (Ann Harbour, USA), all Proteinsimple consumables and reagents were purchased from ProteinSimple (San Jose,California, USA). Baculovirus infected insect cells expressing human UGT isoforms were

purchased from BD Bioscience (Woburn, USA). UGT1A was obtained from Santa Cruz Biotechnology (Dallas, USA), GAPDH, Na^+/K^+ ATPase and α-actinin were from Cell Signaling Technologies (New England Biolabs, Herts, UK). Secondary antibodies for SIMON and WES ProteinSimple were provided by ProteinSimple and used neat. The Caco-2 cell line (HTB-37) and the HepG2 cell line (HB-8065) were obtained from American Type Culture Collection (ATCC) (Manassas, USA), the HT29-MTX cell line (38) was a generous gift from the Nestlé Research Center (Lausanne, Switzerland).

Cell culture

Caco-2 and HT29-MTX cells were routinely cultured in low glucose Dulbecco's Modified Eagle's Medium (DMEM) supplemented with 15% Fetal Bovine Serum (FBS) for Caco-2 and 10% FBS for HT29-MTX, 100 units/mL penicillin, 0.1 mg/mL streptomycin and 0.25 µg/mL Amphotericin B (full medium) at 37°C with 5% CO_2 in a humidified atmosphere. Cells were subcultured when reaching ~ 90% confluency and seeded into flasks at 1 x 10^4 cm^{-2}. For metabolism experiments and surface biotinylation, cells were seeded onto Corning transwell plates of 4.67 cm^2 growth area (Lowell, USA) at a ratio of 24:76 HT29-MTX:Caco-2 and a seeding density of 6 x 10^4 cm^{-2}, unless stated otherwise. Both cell lines were maintained in full medium containing 10% FBS and 50 µM fatty acid dissolved in ethanol (final concentration 0.5%) or the corresponding amount of solvent for controls during their entire differentiation time of 21 days. Cells supplemented with DHA or EPA and their controls were also incubated with 100 µM of the antioxidant α-tocopherol. The medium was replaced every other day. For gene expression studies and protein quantification, cells were seeded onto 6-well plastic plates.

HepG2 cells were grown in Minimum Essential Medium (MEM) supplemented with 10% FBS, non-essential amino acids, 100 µM sodium pyruvate, 100 units/mL penicillin and 0.1 mg/mL streptomycin. Cells were seeded on 6-well plastic plates at a seeding density of 1 x 10^5 cm^{-2}.

Metabolism experiments

On day 22 or day 5 after seeding (Caco-2/HT29-MTX or HepG2 respectively), cells were washed twice with HBSS and if grown on permeable supports, transepithelial electrical resistance (TEER) was measured using a Millicell ERS Ohm meter in HBSS + 1.8 mM Ca^{2+}. The average TEER of co-cultures grown in 6-well transwell plates was 300 Ω. Cell layers were incubated with 200 µM (-)-epicatechin and 100 µM ascorbic acid dissolved in HBSS + 1.8 mM Ca^{2+} either for 120 min (HepG2) or for 90 min from apical or basolateral side (co-cultures and HT29-MTX cells).

Epicatechin metabolite analysis by LC-MS/MS

After incubation of cells with epicatechin, 1.5 mL of the transport buffer was removed, acidified with 100 mM acetic acid, mixed with 50 µM of the internal standard 3,4-dimethoxycinnamic acid and 100 µM ascorbic acid. Cell layers were then washed three times with HBSS and lysed with 80% methanol containing 100 µM ascorbic acid and 5 µM internal standard. Cells were then scraped, collected with the lysate and vortexed vigorously. The lysate was then centrifuged and the supernatant dried under vacuum and reconstituted in 100 µL solvent A.

For LC-MS/MS analysis of epicatechin metabolites, separation was achieved with an Agilent 1200 series HPLC on a Phenomenex Kinetex C18 column (2.6 µm, 150 x 2.1 mm) and 10 µL sample injection. Solvent A consisted of 95% MilliQ water, 5% acetonitrile and 0.5% formic acid. Solvent B consisted of 95% acetonitrile, 5% MilliQ water and 0.5% formic acid. The flow rate was 0.4 mL/min. The solvent gradient started at 0% B for 3 min, a linear increase to 50% solvent B from 3 to 16 min, 100% solvent B for 4 min and return to 0% solvent B at 23 min (39). Epicatechin aglycone and conjugates were detected with an Agilent 6410 triple quadrupole LC-MS/MS in negative MRM mode for the following transitions:

epicatechin (m/z = 289 → 245),
methyl-epicatechin (m/z = 303 → 165),
epicatechin-sulfate (m/z = 369 → 289),
epicatechin-glucuronide (m/z = 465 → 289),
methyl-epicatechin-sulfate (m/z = 383 → 303),
methyl-epicatechin-glucuronide (m/z = 479 → 303).

Identification of metabolite stereoisomers was achieved by comparison with previous publications where authentic standards were available. Actis-Goretta et al. employed very similar chromatography conditions as described

here, and therefore peaks in the present study were identified accordingly (40).

For estimation of relative concentration, the volume of the HT29-MTX cell monolayer was calculated using immunofluorescence (IF) staining of the cell membrane as detailed below. The distance between apical and basolateral membrane was measured by confocal microscopy and was an average of 15 µm estimated from 24 independent experiments. With a growth area of 4.67 cm^2 for transwell plates and 9.5 cm^2 for solid 6-well plates, the volume of a cell monolayer was calculated as 7 and 14 µL respectively.

Protein analysis by capillary electrophoresis in nano-capillaries

For UGT1A protein detection, HT29-MTX cells grown on solid supports were washed with ice cold PBS, scraped and lysed in RIPA buffer containing 0.5% protease inhibitor cocktail by gently rocking the samples on ice for 30 min. The lysate was centrifuged at 14,000 x g for 10 min and the total protein concentration of the supernatant was determined by BCA microplate assay according to the manufacturer's instructions. For the biotinylation and pull down experiments, UGT1A protein abundance was determined using the ProteinSimple system 'SIMON' according to the manufacturer's instructions with the following modifications: loading time of the stacking matrix was increased to 17.0 s, loading time of the sample was increased to 12.0 s and separation time to 47.0 min. Samples were denatured by incubation with sample buffer at room temperature for 30 min. All primary antibodies were used at a dilution of 1:100. For analysis of UGT1A protein level after DHA treatment, the ProteinSimple system 'WES' was used according to standard protocol while the primary antibody incubation was extended to 1 h. α-actinin (1:200) was used as a loading control in the same capillary with UGT1A (1:100). A standard curve was constructed with different amounts of cell lysate to test linearity of both antibodies and loading sample concentration; 0.08 mg/ml was found optimal for signals of both antibodies (Supplementary information). Quantification of peak areas and gel image reconstruction was carried out using ProteinSimple Compass software. Three molecular weight fluorescent standards, incorporated with every sample, were run in every capillary and used to assign the molecular weights to the corresponding peaks.

Cell surface biotinylation and pull down

HT29-MTX cells grown on permeable supports were washed twice with ice cold PBS and incubated with 0.25 mg/mL EZ-Link Sulfo-NHS-LC-Biotin dissolved in HBSS+1.8 mM $CaCl_2$ from either apical or basolateral side. After 4 h of incubation on ice the reaction was stopped by addition of 40 mM Tris to quench the remaining Sulfo-NHS-LC-Biotin. Cells were washed twice with Tris-Buffered Saline (TBS) and lysed with RIPA buffer containing 0.5% protease inhibitor cocktail. After rocking on ice for 20 min, lysates were centrifuged at 14,000xg for 10 min and the supernatant was incubated with 25 µL High Capacity Streptavidin Agarose Resin overnight at 8°C with constant gentle shaking. The supernatant was removed, the resin washed three times with TBS and samples were eluted in 20 µL of 4x ProteinSimple sample buffer containing 0.2 M DTT. 10 µL of sample was used for analysis by capillary electrophoresis as described above.

Immunofluorescence staining and microscopy

HT29-MTX cells were seeded onto Millicell cell culture inserts (12-well, PET 0.4 µm pore size, Millipore) at a density of 6×10^4 cm^{-2} and maintained for 21 days. For staining, cells were fixed with 4% para-formaldehyde in PBS, permeabilized with 0.1% Triton-X100 and incubated with UGT1A (sc-25847) and MRP1 (sc-18835) antibody at a dilution of 1:50 for 1 h. After washing with PBS, cells were further incubated with Alexa488-conjugated donkey anti-rabbit IgG and Cy™3-conjugated donkey anti-mouse IgG obtained from Jackson Immuno Research (West Grove, USA) at a 1:300 dilution. Alternatively, to visualize endoplasmic reticulum, calnexin primary antibody (sc-6465) was used at 1:20 dilution followed by Alexa488-conjugated donkey anti-goat secondary antibody. In these experiments, UGT1A was simultaneously detected using the sc-23847 primary antibody and Cy™3-conjugated donkey anti-rabbit IgG. After that, cell layers were stained with 0.2 µg/mL DAPI and mounted on microscope slides with ProLong Gold antifade reagent mounting medium (Molecular Probes, Carlsbad, USA). Cells were imaged using Zeiss LSM510 or LSM700 confocal microscope.

Widefield images of Caco-2/HT29-MTX co-cultures were acquired using the Leica EL6000

microscope. Percentage of each cell line in the monolayer at day 21 was calculated from widefield images using the ImageJ software (NIH, USA).

Gene expression analysis

Cells were seeded onto solid supports at 6×10^4 cm^{-2} and maintained in full medium supplemented with DHA or vehicle for 22 days (Caco-2 and HT29-MTX) or 5 days (HepG2). Cells were washed with HBSS, scraped and mRNA was extracted using the Ambion RNAqueous kit from Life Technologies (Carlsbad, USA), according to the manufacturer's protocol. RNA (1 µg) was transcribed to cDNA using the Applied Biosystems high capacity RNA to cDNA kit. 100 ng cDNA were used to analyze gene expression by TaqMan real-time PCR using Applied Biosystems TaqMan gene expression assays and TaqMan gene expression master mix according to the manufacturer's protocol on a StepOnePlus Real-Time PCR system. GAPDH was used as reference (NM_002046.3, VIC/MGB_PL, 4326317E).

Absolute quantification of UGT1A isoforms in HT29-MTX cells

The QX100 Droplet Digital PCRsystem (BioRad Laboratories Inc, Hercules, CA) was used to quantify expression of different UGT1A isoforms in HT29-MTX cells from 3 biological replicates in 3 seeding experiments (total n=9), with 3 technical replicates (total n=27). mRNA was extracted as above and following DNAse treatment (TURBO DNA-free Kit, Ambion, Life Technologies) to exclude genomic DNA contamination, 1 µg was transcribed to cDNA as above. 0.65 ng of transcribed DNA diluted with Milli-Q water to 9 µl was introduced in every 20 µl assay/well including 1 µl of UGT FAM labelled TaqMan primer (Life Technologies) and 10 µL ddPCR Supermix for Probes (BioRad). Droplets were generated according to manufacturer guidelines with the QX100 Droplet generator (BioRad) before cycling in a C1000 Touch thermal cycler (BioRad) at optimal temperature for every primer for 30 min, followed by 95 °C (10 min), 40 cycles of 94 °C (0.5 min) followed by 60 °C (60 min), 98 °C (10 min). Plates were held at 12 °C between amplification and droplet reading. On average ddPCR yielded a number of 14,098 accepted droplets with a standard deviation of 972 droplets. Data from the QX100 Droplet Reader were analyzed with the QuantaSoft software (Kosice, Slovakia). Fluorescent droplets were deemed positive by automatically set thresholds and concentration of the target DNA in copies per microliter was calculated from the fraction of positive reactions using Poisson distribution analysis.

In vitro glucuronidation assay

Activity of different UGT isoforms towards epicatechin was tested using recombinant human enzymes expressed in insect microsomes. In vitro glucuronidation assay was performed as described by Wong et al., 2010 (41).

Statistics

Statistical analysis was conducted with SPSS v22. Values shown are the mean of n independent experiments ± standard error of the mean unless otherwise indicated. For analysis of statistically significant differences, unpaired Students t-test was used.

RESULTS

Highest UGT activity has been found in the liver and so the HepG2 hepatic cell line was first used to investigate the effect of chronic supplementation with different fatty acids on glucuronidation rate (Figure 1). Stearic acid (C18:0) had no effect on metabolite formation while PUFA increased glucuronidation as assessed by formation of the most abundant metabolite epicatechin-3´-glucuronide (EC-3´-glc). EPA (C20:5) increased only intracellular EC-3´-glc levels while α-linolenic acid (C18:3), arachidonic acid (C20:4) and DHA (C22:6) increased both intra- and extracellular EC-3´-glc concentrations.

Apart from the liver, the small intestine has also been shown to have high capacity for glucuronidation. Therefore, a cell culture model of the small intestine was chosen to further investigate the impact of fatty acid pre-treatment on glucuronic acid conjugation. DHA increased conjugation rates 2-fold in HepG2 cells and was therefore selected to assess glucuronidation in the Caco-2/HT29-MTX co-culture model. Cells were treated with DHA for their entire differentiation time of 22 days and controls were treated with vehicle only. Figure 2 shows the relative concentration of several epicatechin metabolites compared to the total amount in different compartments of the cell model. All glucuronide isomers showed the same pattern of distribution:

the highest concentration was found intracellularly and the highest amount was found in the basolateral well when substrate was applied basolaterally. Surprisingly there was a dramatic ~50-fold difference depending on whether substrate was applied to the apical or basolateral side. DHA treatment was able to further increase glucuronide levels up to 4-fold in all compartments. None of the products from the other conjugating enzymes sulfotransferase (SULT) and catechol-O-methyltransferase (COMT) exhibited the same pattern of distribution as glucuronides. Figure 2 shows representative graphs for the most abundant metabolites 3´-methyl-epicatechin (3´-meEC), epicatechin-3´-sulfate (EC-3´-sulf) and 3´-methyl-epicatechin-7-sulfate (3´-EC-7-sulf). For all these compounds the highest concentration was found intracellularly, but unlike for the glucuronic acid conjugates, the highest amount was not detected in samples from the basolateral well but in cell lysates. Aglycone applied to the basolateral side resulted in 5-fold higher concentrations of sulfate- and methyl-conjugates than aglycone applied to the apical side but this difference is small in comparison to the 50- fold difference observed with glucuronic acid conjugates. The methyl-sulfate double conjugate even showed converse distribution, with 5-fold higher amounts detected when epicatechin was applied apically. None of the non-glucuronide metabolites demonstrated a pronounced difference in apical and basolateral distribution, indicating that these conjugates are not preferentially transported to the side of aglycone application, in contrast to the effect observed with glucuronides. DHA treatment had no impact on the activity of COMT or SULT, in contrast with UGT. The fact that DHA increased the amount of only one type of metabolite shows that there is a specific effect of DHA on that enzyme and it is not a generic mechanism that is altered. Also the striking difference in glucuronide production depending on the aglycone transport direction (a → b vs. b → a) is unique to UGT products and so does not stem from an increased uptake of epicatechin and consequent increase in substrate availability from the basolateral side, since then the concentration of SULT and COMT products would also have been increased. Therefore, UGT shows a unique pattern of activity which is asymmetrically distributed within the cell and responds to DHA supplementation. The existing model of an enzyme solely residing in the ER cannot explain the observations presented here.

The Caco-2/HT29-MTX seeding ratio of 76/24, used for the transport experiments, was chosen to represent the percentage of goblet cells in the small intestine. Because Caco-2 cells grow faster than HT29-MTX cells, seeding 24% goblet cells typically resulted in 13 ± 2% goblet cells in the monolayer after differentiation, growing as patches of Caco-2 cells with ribbons of HT29-MTX running through (Figure 3A). To investigate whether the seeding ratio of the two cell lines has an impact on glucuronidation activity, different ratios were tested. Figure 3B shows the impact of increasing amounts of HT29-MTX cells in the model on glucuronic acid conjugation rates. There is an almost linear relationship between EC-3´-glc production and the percentage of goblet cells seeded. This indicates that Caco-2 cells make only a minor contribution to the overall glucuronidation rate and that either the activity or the abundance of UGT isoforms is much greater in HT29-MTX cells.

The UGT isoforms which catalyze glucuronidation of epicatechin are not known so recombinant human UGTs expressed in insect microsomes were used to determine specificity. Three UGTs of the 1A family showed significant activity towards epicatechin: UGT1A1, UGT1A8 and UGT1A9 (Figure 4). Consistent with epicatechin metabolism by liver and intestinal cells, EC-3´-glc was produced with the highest rate, followed by EC-7-glc and then EC-4´-glc.

Gene expression of the relevant isoforms UGT1A1, UGT1A8 and UGT1A9 was investigated in HepG2, Caco-2 and HT29-MTX cells. Figure 5A shows their relative mRNA abundance normalised to the housekeeping gene GAPDH. For all three UGT isoforms similar mRNA levels were found in Caco-2 and HepG2 cells. Absolute quantification of all UGT1A isoforms in HT29-MTX cells (Table 1) showed ~ 100 fold higher levels of UGT1A8 and 1A10 mRNA compared to 1A1, 1A3, 1A7 and 1A9, and 10-fold higher than UGT1A6. Since UGT1A8 has the highest activity on epicatechin, this isoform is predicted to be the dominant epicatechin conjugating UGT in Caco-2/HT29-MTX co-cultures. The impact of chronic DHA treatment on UGT gene expression was measured after 21 day

treatment in Caco-2 and HT29-MTX cells grown separately and after 5 day treatment in HepG2 cells. UGT1A1 expression was upregulated in Caco-2 and HT29-MTX cells and UGT1A8 was upregulated in HT29-MTX and HepG2 cells. UGT1A9 was not affected by DHA treatment (figure 5B).

As no specific UGT1A8 antibody was commercially available, the impact of DHA on protein levels of UGT1A8 in HT29-MTX cells was assessed using a generic UGT1A antibody recognising all isoforms of that family. However, having shown that in that cell line UGT1A8 and 1A10 are much more abundant than the other UGTs investigated, we predicted confidently that the UGT1A detected by that antibody will be mainly UGT1A8 and 1A10. The antibody characteristics and dose-response are shown in Figure 6. Using this quantification with a-actinin as internal standard, we show that UGT1A levels increased by 70% with chronic DHA treatment in HT29-MTX whole cell lysates (Figure 7).

As discussed above, the metabolic pattern indicates that there might be a more complex mechanism to substrate glucuronidation by UGT1A8 than the model of an ER membrane residing enzyme. Figure 8 shows that UGT1A(8/10) was detected in the plasma membrane, co-localizing with the plasma membrane marker MRP1. The signal was stronger in lateral and basal membranes than on the apical side. Calnexin staining was used to visualise the ER which was distributed evenly throughout the cell, and only partially overlapped with the UGT1A(8/10) staining (Figure 8, panel F). So far, most UGT isoforms have been described to localize to the ER. Goblet cells have a unique structure with most of the apical lumen being filled with mucus containing granules and the basolateral lumen holding the nucleus. This conformation leaves little room for cytosolic organelles like the Golgi and the ER, which are consequently very much localized in the peripheral space of the cell, close to the plasma membrane. Considering this spatial peculiarity, it might be that the apparent co-localization of UGT and membrane marker MRP1 is due to the ER residing UGT being localized just below the plasma membrane (42).

To confirm whether UGT1A(8/10) really is plasma membrane spanning in HT29-MTX cells, cell surface biotinylation and pull down with streptavidin resin was performed. UGT1A(8/10) protein was detected on the apical and basolateral surface of HT29-MTX cells grown on permeable supports (Figure 9). The enzyme was more abundant in the lysate from cells incubated with biotin labelled from the basolateral side than in lysate of cells labelled from the apical side. Intracellular protein GAPDH was used as a negative control to monitor cell membrane integrity during biotinylation and plasma membrane spanning Na^+/K^+-ATPase was used as a positive control for successful biotinylation and pull down. No GAPDH could be detected in the apical surface lysate, which confirms the presence of UGT1A in the plasma membrane.

The results described above show that at least some of the UGT1A(8/10) pool is plasma membrane spanning in HT29-MTX cells. It is not clear however, what the orientation of the enzyme in the plasma membrane is. If it was inserted the same way as into the ER membrane, the enzyme's active site would be facing the extracellular space. If it was inserted the opposite way, the cytoplasmic tail would be outside the cell. In the first case, with the active site facing the extracellular space, the availability of the co-factor UDPGA would be the rate-limiting step of the enzyme reaction. High concentrations of substrate are in contact with the cell surface in transport experiments but the co-factor would have to be exported from the cytosol to reach the active site of the enzyme. To test whether the active site is exposed to the extracellular space, the glucuronidation rate of substrate epicatechin was measured with and without externally supplied co-factor. Adding UDPGA externally did not increase EC-3´-glc levels in either the supernatant or the cytosol (Figure 10), indicating that the UDPGA binding site of the enzyme is not exposed on the cell surface.

DISCUSSION

Previous studies that examined the effect of fatty acids on glucuronidation, using microsomes or animal models, have generated diverse conclusions. In the current study, chronic fatty acid supplementation was used to elucidate the impact of lipids on glucuronic acid conjugation, using epicatechin as a model substrate. Epicatechin was preferentially glucuronidated by UGT1A9, which is mainly

expressed in liver, and also by UGT1A8 which is extrahepatic and mainly expressed in the small intestine but also in kidney (29,43-47). In the intestinal Caco-2/HT29-MTX model, UGT1A8 and 1A10 were the most abundant isoforms. UGT1A8 expression was much higher in HT29-MTX than in Caco-2 cells. In the small intestine, UGT1A1 and UGT1A10 are the dominant isoforms of the UGT1A family (20,48). HT29-MTX cells are goblet cells, one of five different cell types present in the intestine where it only amounts to 10 to 15% of the mucosa (49). In total mRNA extracts of intestinal tissue samples, the expression pattern of enterocytes would be predominant as those are the major cell type present in that tissue.

Hitherto it has not been reported how the gene expression profile of enzymes involved in phase II metabolism varies in the different intestinal cell types. Goblet cells are generally not thought to be extensively involved in nutrient and xenobiotic metabolism. Their main function is to produce and excrete mucus that will act as a diffusion barrier and protect the intestinal epithelium from pathogen invasion, mechanical stress and injury (50). However, it is possible that some UGT isoforms may serve an alternative function in mucus secreting cells than in enterocytes, as seen for SULTs. SULTs also conjugate xenobiotics in most cell types, but in goblet cells they sulfonate mucin molecules. The increase of SULT protein along the length of the intestine results in elevated acidity of the intestinal mucus layer towards the colon (51-53).

In metabolism experiments, using the Caco-2/HT29-MTX co-culture, a previously unseen distribution pattern of glucuronic acid conjugates was observed which was due to the glucuronidation activity of the HT29-MTX cells. There were considerable differences in conjugation rate depending on the transport direction. When the aglycone was applied to the apical side of the cell layer, which in vivo corresponds to UGT substrate reaching the intestinal mucosa from the gut lumen, glucuronidation was much lower than when aglycone was applied to the basolateral side, which in vivo would correspond to UGT substrate taken up into the mucosa from the submucosa. Glucuronides were preferentially transported to the side of epicatechin application. These observations fit well with results obtained by indirect immunofluorescence staining of HT29-MTX cells for UGT1A as high levels of UGT1A were observed in the lateral and basal parts of the plasma membrane. We hypothesize that after entering the cell, the substrate is readily glucuronidated by UGT localized at the plasma membrane and quickly exported to the extracellular space by basolaterally located efflux transporters. When substrate was applied to the basolateral side, 95% of EC-3´-glc produced was transported to the basolateral compartment. Such highly efficient efflux of product suggests that EC-glc is an potential allocrite of a transporter located in the immediate vicinity of the enzyme (Figure 11). All UGT isoforms contain a signal peptide at the N-terminus, which targets the nascent protein to the ER, and a C-terminal ER retention signal. The signal peptide is cleaved off after insertion of the protein into the ER membrane. However, it is still not entirely clear which sequence elements retain the UGT protein in the ER. It has been shown that the transmembrane domain (TMD) and the cytosolic tail (CT) act as stop sequences that anchor the enzyme in the ER membrane and that the cytosolic tail contains a retrieval signal that targets any escaped protein for transport from the Golgi back to the ER. When TMD and CT were fused with the extracellular domain of CD4, this plasma membrane protein became ER resident (54). On the other hand, neither deleting the N-terminal signal peptide nor removing the CT and TMD had an impact on UGT1A6 ER localization. Instead it was the internal membrane anchoring region that played a vital role in ER localization of that UGT enzyme (55,56).

Some reports have also detected UGT protein or activity in the nuclear envelope and the Golgi (57-59). Early studies even found UGT activity in the plasma membrane of liver cells (60-62). In the present study, a stronger signal and activity was associated with the basolateral membrane, whereas in another report with similar staining pattern of intestinal tissue samples, the strongest signal was towards the apical surface of crypt cells (63,64). The presence of the mucus layer produced by HT29-MTX cells could restrict diffusion of the antibody to the apical but not the basolateral cell surface, in comparison to intestinal

samples which are sliced and stained along the lateral axis.

All UGT1A isoforms are alternative splice variants from a single gene locus with only the first, N-terminal exon being unique for each isoform and exons 2-5 being shared among all UGT1A forms. A number of Single Nucleotide Polymorphisms (SNPs) have been reported for all UGT isoforms. Eight different mutations have been described for UGT1A8, leading to three allelic variants. All three alleles were cloned and expressed in HEK293 cells but none of them localized in the plasma membrane (65). One mutation in the signal peptide region ($T^{4}A$) of UGT1A8 has been reported but not cloned and expressed in vitro (66). Several studies observed that the enzymes translated from the three different alleles had different glucuronidation activity. UGT1A8*1 and UGT1A8*2 ($A^{173}G$) have similar activity whereas UGT1A8*3 ($C^{277}Y$) only shows very low activity (9,65) and has been identified as a risk factor in colorectal cancer (67). UGT1A8*3 occurs with low frequency in the general population but is much more abundant in tumour cells. Since most cell lines are carcinoma derived, such increased abundance of this low activity allele might help to explain some inconsistencies between in vivo and in vitro results.

Fatty acids have previously been shown to upregulate expression of some UGTs in vivo. Interestingly, DHA treatment increased expression of UGT1A8 in HepG2 and HT29-MTX cells but not of UGT1A9, even though DHA has been shown to increase PPARα activity in Caco-2 cells (68) and UGT1A9 expression was shown to be upregulated with increased PPARα activity (32).
In summary, it was shown that HT29-MTX cells display a unique distribution of UGT1A8/10 protein in the plasma membrane, with UGT1A8 showing a functional catalytic localization to the basolateral membrane. Further studies will have to show whether this is a common feature of mucus cells that has so far been overlooked because most studies on UGT activity and localization have been conducted using liver cells where that particular isoform is not expressed.

REFERENCES

1. Rouleau, M., Collin, P., Bellemare, J., Harvey, M., and Guillemette, C. (2013) Protein-protein interactions between the bilirubin-conjugating UDPglucuronosyltransferase UGT1A1 and its shorter isoform 2 regulatory partner derived from alternative splicing. *Biochemical Journal* **450**, 107-114
2. Rowland, A., Miners, J. O., and Mackenzie, P. I. (2013) The UDP-glucuronosyltransferases: Their role in drug metabolism and detoxification. *International Journal of Biochemistry & Cell Biology* **45**, 1121-1132
3. Grosse, L., Campeau, A.-S., Caron, S., Morin, F.-A., Meunier, K., Trottier, J., Caron, P., Verreault, M., and Barbier, O. (2013) Enantiomer Selective Glucuronidation of the Non-Steroidal Pure Anti-Androgen Bicalutamide by Human Liver and Kidney: Role of the Human UDP-Glucuronosyltransferase (UGT)1A9 Enzyme. *Basic & Clinical Pharmacology & Toxicology* **113**, 92-102
4. Gill, K. L., Houston, J. B., and Galetin, A. (2012) Characterization of In Vitro Glucuronidation Clearance of a Range of Drugs in Human Kidney Microsomes: Comparison with Liver and Intestinal Glucuronidation and Impact of Albumin. *Drug Metabolism and Disposition* **40**, 825-835
5. Malfatti, M. A., Wu, R. W., and Felton, J. S. (2005) The effect of UDP-glucuronosyltransferase 1A1 expression on the mutagenicity and metabolism of the cooked-food carcinogen 2-amino-1-methyl-6-phenylimidazo 4,5-b pyridine in CHO cells. *Mutation Research-Fundamental and Molecular Mechanisms of Mutagenesis* **570**, 205-214
6. Leung, H. Y., Wang, Y., and Leung, L. K. (2007) Differential effect of over-expressing UGT1A1 and CYP1A1 on xenobiotic assault in MCF-7 cells. *Toxicology* **242**, 153-159
7. Xu, L., Krenitsky, D. M., Seacat, A. M., Butenhoff, J. L., Tephly, T. R., and Anders, M. W. (2006) N-glucuronidation of perfluorooctanesulfonamide by human, rat, dog, and monkey liver microsomes and by expressed rat and human UDP-glucuronosyltransferases. *Drug Metabolism and Disposition* **34**, 1406-1410
8. Jenkinson, C., Petroczi, A., and Naughton, D. P. (2013) Effects of Dietary Components on Testosterone Metabolism via UDP-Glucuronosyltransferase. *Frontiers in endocrinology* **4**, 80-80
9. Thibaudeau, J., Lepine, J., Tojcic, J., Duguay, Y., Pelletier, G., Plante, M., Brisson, J., Tetu, B., Jacob, S., Perusse, L., Belanger, A., and Guillemette, C. (2006) Characterization of common UGT1A8, UGT1A9, and UGT2B7 variants with different capacities to inactivate mutagenic 4-hydroxylated metabolites of estradiol and estrone. *Cancer Research* **66**, 125-133
10. Kato, Y., Ikushiro, S.-i., Emi, Y., Tamaki, S., Suzuki, H., Sakaki, T., Yamada, S., and Degawa, M. (2008) Hepatic UDP-glucuronosyltransferases responsible for glucuronidation of thyroxine in humans. *Drug Metabolism and Disposition* **36**, 51-55
11. Cheng, Z. Q., Radominska-Pandya, A., and Tephly, T. R. (1999) Studies on the substrate specificity of human intestinal UDP-glucuronosyltransferases 1A8 and 1A10. *Drug Metabolism and Disposition* **27**, 1165-1170
12. Jimenez, R., Duarte, J., and Perez-Vizcaino, F. (2012) Epicatechin: Endothelial Function and Blood Pressure. *Journal of Agricultural and Food Chemistry* **60**, 8823-8830
13. Wu, B., Kulkarni, K., Basu, S., Zhang, S., and Hu, M. (2011) First-Pass Metabolism via UDP-Glucuronosyltransferase: a Barrier to Oral Bioavailability of Phenolics. *Journal of Pharmaceutical Sciences* **100**, 3655-3681
14. Ng, S. P., Wong, K. Y., Zhang, L., Zuo, Z., and Lin, G. (2005) Evaluation of the first-pass glucuronidation of selected flavones in gut by Caco-2 monolayer model. *Journal of Pharmacy and Pharmaceutical Sciences* **8**, 1-9

15. Singh, R., Wu, B., Tang, L., and Hu, M. (2011) Uridine Diphosphate Glucuronosyltransferase Isoform-Dependent Regiospecificity of Glucuronidation of Flavonoids. *Journal of Agricultural and Food Chemistry* **59**, 7452-7464
16. Wong, C. C., Barron, D., Orfila, C., Dionisi, F., Krajcsi, P., and Williamson, G. (2011) Interaction of hydroxycinnamic acids and their conjugates with organic anion transporters and ATP-binding cassette transporters. *Molecular Nutrition & Food Research* **55**, 979-988
17. Trottier, J., Verreault, M., Grepper, S., Monte, D., Belanger, J., Kaeding, J., Garon, P., Inaba, T. T., and Barbier, O. (2006) Human UDP-glucuronosyltransferase (UGT)1A3 enzyme conjugates chenodeoxycholic acid in the liver. *Hepatology* **44**, 1158-1170
18. Levesque, B., Beaulieu, M., Hum, D. W., and Belanger, A. (1999) Characterization and substrate specificity of UGT2B4 (E-458): a UDP-glucuronosyltransferase encoded by a polymorphic gene. *Pharmacogenetics* **9**, 207-216
19. Meech, R., Miners, J. O., Lewis, B. C., and Mackenzie, P. I. (2012) The glycosidation of xenobiotics and endogenous compounds: Versatility and redundancy in the UDP glycosyltransferase superfamily. *Pharmacology & Therapeutics* **134**, 200-218
20. Ohno, S., and Nakajin, S. (2009) Determination of mRNA Expression of Human UDP-Glucuronosyltransferases and Application for Localization in Various Human Tissues by Real-Time Reverse Transcriptase-Polymerase Chain Reaction. *Drug Metabolism and Disposition* **37**, 32-40
21. Zakim, D., Goldenbe.J, and Vessey, D. A. (1973) Influence of Membrane Lipids on Regulatory Properties of UDP-Glucuronyltransferase. *European Journal of Biochemistry* **38**, 59-63
22. Zakim, D. (1970) Regulation of Microsomal Enzymes by Phospholipids: 1. Effect of Phospholipases and Phospholipids on Glucose-6-Phosphatase. *Journal of Biological Chemistry* **245**, 4953-&
23. Vessey, D. A., and Zakim, D. (1971) Regulation of Microsomal Enzymes by Phospholipids: 2. Activation of Hepatic Uridine Diphosphate-Glucuronyltransferase. *Journal of Biological Chemistry* **246**, 4649-&
24. Dannenberg, A. J., and Zakim, D. (1992) Dietary Lipid Regulates the Amount and Functional State of UDP-Glucuronosyltransferase in Rat Liver. *Journal of Nutrition* **122**, 1607-1613
25. Dannenberg, A. J., Yang, E. K., and Aharon, D. (1993) Dietary Lipids Induce Phase 2 Enzymes in Rat Small-Intestine. *Biochimica Et Biophysica Acta* **1210**, 8-12
26. Dannenberg, A. J., and Yang, E. K. (1992) Effect of Dietary Lipids on Levels Of UDP-Glucuronosyltransferase in Liver. *Biochemical Pharmacology* **44**, 335-340
27. Kato, J., Ikemoto, A., and Mizutani, T. (2003) The effect of dietary fatty acids on the expression levels and activities of hepatic drug metabolizing enzymes. *Journal of Health Science* **49**, 105-114
28. Abumrad, N. A., and Davidson, N. O. (2012) Role of the Gut in Lipid Homeostasis. *Physiological Reviews* **92**, 1061-1085
29. Okamura, K., Ishii, Y., Ikushiro, S., Mackenzie, P. I., and Yamada, H. (2006) Fatty acyl-CoA as an endogenous activator of UDP-glucuronosyltransferases. *Biochemical and Biophysical Research Communications* **345**, 1649-1656
30. Tsoutsikos, P., Miners, J. O., Stapleton, A., Thomas, A., Sallustio, B. C., and Knights, K. M. (2004) Evidence that unsaturated fatty acids are potent inhibitors of renal UDP-glucuronosyltransferases (UGT): kinetic studies using human kidney cortical microsomes and recombinant UGT1A9 and UGT2B7. *Biochemical Pharmacology* **67**, 191-199
31. Shibuya, A., Itoh, T., Tukey, R. H., and Fujiwara, R. (2013) Impact of fatty acids on human UDP-glucuronosyltransferase 1A1 activity and its expression in neonatal hyperbilirubinemia. *Scientific Reports* **3**

32. Barbier, O., Villeneuve, L., Bocher, V., Fontaine, C., Torra, I. P., Duhem, C., Kosykh, V., Fruchart, J. C., Guillemette, C., and Staels, B. (2003) The UDP-glucuronosyltransferase 1A9 enzyme is a peroxisome proliferator-activated receptor alpha and gamma target gene. *Journal of Biological Chemistry* **278**, 13975-13983
33. Forman, B. M., Chen, J., and Evans, R. M. (1997) Hypolipidemic drugs, polyunsaturated fatty acids, and eicosanoids are ligands for peroxisome proliferator-activated receptors alpha and delta. *Proceedings of the National Academy of Sciences of the United States of America* **94**, 4312-4317
34. Kliewer, S. A., Sundseth, S. S., Jones, S. A., Brown, P. J., Wisely, G. B., Koble, C. S., Devchand, P., Wahli, W., Willson, T. M., Lenhard, J. M., and Lehmann, J. M. (1997) Fatty acids and eicosanoids regulate gene expression through direct interactions with peroxisome proliferator-activated receptors alpha and gamma. *Proceedings of the National Academy of Sciences of the United States of America* **94**, 4318-4323
35. Vaidyanathan, J. B., and Walle, T. (2002) Glucuronidation and sulfation of the tea flavonoid (-)-epicatechin by the human and rat enzymes. *Drug Metabolism and Disposition* **30**, 897-903
36. Stalmach, A., Mullen, W., Steiling, H., Williamson, G., Lean, M. E. J., and Crozier, A. (2010) Absorption, metabolism, and excretion of green tea flavan-3-ols in humans with an ileostomy. *Molecular Nutrition & Food Research* **54**, 323-334
37. Auger, C., Mullen, W., Hara, Y., and Crozier, A. (2008) Bioavailability of polyphenon E flavan-3-ols in humans with an ileostomy. *The Journal of nutrition* **138**, 1535S-1542S
38. Lesuffleur, T., Barbat, A., Dussaulx, E., and Zweibaum, A. (1990) Growth adaptation to methotrexate of ht-29 human colon-carcinoma cells is associated with their ability to differentiate into columnar absorptive and mucus-secreting cells. *Cancer Research* **50**, 6334-6343
39. Clarke,K.A., Dew,T.P., Watson,R.E., Farrar,M.D., Bennett,S., Nicolaou,A., Rhodes,L.E., and Williamson,G. (2014) High performance liquid chromatography tandem mass spectrometry dual extraction method for identification of green tea catechin metabolites excreted in human urine. *J.Chromatogr.B.*, **972**, 29-37.
40. Actis-Goretta, L., Leveques, A., Giuffrida, F., Romanov-Michailidis, F., Viton, F., Barron, D., Duenas-Paton, M., Gonzalez-Manzano, S., Santos-Buelga, C., Williamson, G., and Dionisi, F. (2012) Elucidation of (-)-epicatechin metabolites after ingestion of chocolate by healthy humans. *Free Radical Biology and Medicine* **53**, 787-795
41. Wong, C. C., Meinl, W., Glatt, H.-R., Barron, D., Stalmach, A., Steiling, H., Crozier, A., and Williamson, G. (2010) In vitro and in vivo conjugation of dietary hydroxycinnamic acids by UDP-glucuronosyltransferases and sulfotransferases in humans. *Journal of Nutritional Biochemistry* **21**, 1060-1068
42. Specian, R. D., and Oliver, M. G. (1991) Functional Biology of Intestinal Goblet Cells. *American Journal of Physiology* **260**, C183-C193
43. Fallon, J. K., Neubert, H., Hyland, R., Goosen, T. C., and Smith, P. C. (2013) Targeted Quantitative Proteomics for the Analysis of 14 UGT1As and-2Bs in Human Liver Using NanoUPLC-MS/MS with Selected Reaction Monitoring. *Journal of Proteome Research* **12**, 4402-4413
44. Izukawa, T., Nakajima, M., Fujiwara, R., Yamanaka, H., Fukami, T., Takamiya, M., Aoki, Y., Ikushiro, S.-i., Sakaki, T., and Yokoi, T. (2009) Quantitative Analysis of UDP-Glucuronosyltransferase (UGT) 1A and UGT2B Expression Levels in Human Livers. *Drug Metabolism and Disposition* **37**, 1759-1768
45. Sato, Y., Nagata, M., Tetsuka, K., Tamura, K., Miyashita, A., Kawamura, A., and Usui, T. (2014) Optimized methods for targeted Peptide-based quantification of human uridine 5'-diphosphate-glucuronosyltransferases in biological specimens using liquid

chromatography-tandem mass spectrometry. *Drug metabolism and disposition: the biological fate of chemicals* **42**, 885-889
46. Hanioka, N., Nonaka, Y., Saito, K., Negishi, T., Okamoto, K., Kataoka, H., and Narimatsu, S. (2012) Effect of aflatoxin B1 on UDP-glucuronosyltransferase mRNA expression in HepG2 cells. *Chemosphere* **89**, 526-529
47. Harbourt, D. E., Fallon, J. K., Ito, S., Baba, T., Ritter, J. K., Glish, G. L., and Smith, P. C. (2012) Quantification of Human Uridine-Diphosphate Glucuronosyl Transferase 1A Isoforms in Liver, Intestine, and Kidney Using Nanobore Liquid Chromatography-Tandem Mass Spectrometry. *Analytical Chemistry* **84**, 98-105
48. Court, M. H., Zhang, X., Ding, X., Yee, K. K., Hesse, L. M., and Finel, M. (2012) Quantitative distribution of mRNAs encoding the 19 human UDP-glucuronosyltransferase enzymes in 26 adult and 3 fetal tissues. *Xenobiotica* **42**, 266-277
49. Noah, T. K., Donahue, B., and Shroyer, N. F. (2011) Intestinal development and differentiation. *Experimental Cell Research* **317**, 2702-2710
50. Johansson, M. E. V., Sjovall, H., and Hansson, G. C. (2013) The gastrointestinal mucus system in health and disease. *Nature Reviews Gastroenterology & Hepatology* **10**, 352-361
51. Croix, J. A., Bhatia, S., and Gaskins, H. R. (2011) Inflammatory cues modulate the expression of secretory product genes, Golgi sulfotransferases and sulfomucin production in LS174T cells. *Experimental Biology and Medicine* **236**, 1402-1412
52. Campbell, B. J., Rowe, G. E., Leiper, K., and Rhodes, J. M. (2001) Increasing the intra-Golgi pH of cultured LS174T goblet-differentiated cells mimics the decreased mucin sulfation and increased Thomsen-Friedenreich antigen (Gal beta 1-3GalNac alpha-) expression seen in colon cancer. *Glycobiology* **11**, 385-393
53. Forstner, J., Roomi, N., Khorasani, R., Kuhns, W., and Forstner, G. (1991) Effect of Reserpine on the Histochemical and Biochemical-Properties of Rat Intestinal Mucin. *Experimental and Molecular Pathology* **54**, 129-143
54. Barre, L., Magdalou, J., Netter, P., Fournel-Gigleux, S., and Ouzzine, M. (2005) The stop transfer sequence of the human UDP-glucuronosyltransferase 1A determines localization to the endoplasmic reticulum by both static retention and retrieval mechanisms. *Febs Journal* **272**, 1063-1071
55. Ouzzine, M., Magdalou, J., Burchell, B., and Fournel-Gigleux, S. (1999) An internal signal sequence mediates the targeting and retention of the human UDP-glucuronosyltransferase 1A6 to the endoplasmic reticulum. *Journal of Biological Chemistry* **274**, 31401-31409
56. Ouzzine, M., Magdalou, J., Burchell, B., and Fournel-Gigleux, S. (1999) Expression of a functionally active human hepatic UDP-glucuronosyltransferase (UGT1A6) lacking the N-terminal signal sequence in the endoplasmic reticulum. *Febs Letters* **454**, 187-191
57. Zaleski, J., Bansal, S. K., and Gessner, T. (1982) Nuclear Membrane-Bound UDP-Glucuronsyltransferase of Rat-Liver. *Canadian Journal of Biochemistry* **60**, 972-979
58. Chowdhury, J. R., Novikoff, P. M., Chowdhury, N. R., and Novikoff, A. B. (1985) Distribution Of UDPglucuronosyltransferase in Rat-Tissue. *Proceedings of the National Academy of Sciences of the United States of America* **82**, 2990-2994
59. Hauser, S. C., Ziurys, J. C., and Gollan, J. L. (1984) Subcellular Distribution and Regulation of Hepatic Bilirubin UDP-Glucuronyltransferase. *Journal of Biological Chemistry* **259**, 4527-4533
60. Antoine, B., Magdalou, J., and Siest, G. (1983) Functional-Heterogeneity Of UDP-Glucuronosyltransferases in Different Membranes of Rat-Liver. *Biochemical Pharmacology* **32**, 2629-2632

61. Antoine, B., Magdalou, J., and Siest, G. (1984) Kinetic-Properties of UDP-Glucuronosyltransferase(S) In Different Membranes of Rat-Liver Cells. *Xenobiotica* **14**, 575-579
62. Magdalou, J., Antoine, B., Ratanasavanh, D., and Siest, G. (1982) Phenobarbital Induction of Cytochrome-P-450 And UDP-Glucuronosyltransferase in Rabbit Liver Plasma-Membranes. *Enzyme* **28**, 41-47
63. Strassburg, C. P., Kneip, S., Topp, J., Obermayer-Straub, P., Barut, A., Tukey, R. H., and Manns, M. P. (2000) Polymorphic gene regulation and interindividual variation of UDP-glucuronosyltransferase activity in human small intestine. *Journal of Biological Chemistry* **275**, 36164-36171
64. Strassburg, C. P., Nguyen, N., Manns, M. P., and Tukey, R. H. (1999) UDP-glucuronosyltransferase activity in human liver and colon. *Gastroenterology* **116**, 149-160
65. Huang, Y. H., Galijatovic, A., Nguyen, N., Geske, D., Beaton, D., Green, J., Green, M., Peters, W. H., and Tukey, R. H. (2002) Identification and functional characterization of UDP-glucuronosyltransferases UGT1A8*1, UGT1A8*2 and UGT1A8*3. *Pharmacogenetics* **12**, 287-297
66. Mojarrabi, B., and Mackenzie, P. I. (1998) Characterization of two UDP glucuronosyltransferases that are predominantly expressed in human colon. *Biochemical and Biophysical Research Communications* **247**, 704-709
67. Wang, M., Sun, D.-F., Wang, S., Qing, Y., Chen, S., Wu, D., Lin, Y.-M., Luo, J.-Z., and Li, Y.-Q. (2013) Polymorphic Expression of UDP-Glucuronosyltransferase UGTIA Gene in Human Colorectal Cancer. *Plos One* **8**
68. Kimura, R., Takahashi, N., Lin, S., Goto, T., Murota, K., Nakata, R., Inoue, H., and Kawada, T. (2013) DHA attenuates postprandial hyperlipidemia via activating PPAR alpha in intestinal epithelial cells. *Journal of Lipid Research* **54**, 3258-3268

FOOTNOTES

[a] The Nestlé Research Center Lausanne (Switzerland) provided partial funding for a PhD studentship to KZ. GW, ST and AK are partly funded by an European Research Council Advanced Grant (POLYTRUE? 322467).

[b] Abbreviations used: UGT, UDP-glucuronosyltransferase; DHA, docosahexaenoic acid; PPAR, peroxisome proliferator-activated receptor; RXR, retinoid x receptor; TMD, transmembrane domain; CT, cytosolic tail; COMT, catechol-O-methyltransferase; SULT, sulfotransferase, ec, epicatechin; sulf, sulfate; gluc, glucuronide; me-, methyl; ER, endoplasmic reticulum

FIGURE LEGENDS

FIGURE 1, Effect of PUFAs on EC-3´-glc formation in HepG2 cells. Ratio of EC-3´-glc concentration detected in the supernatant and the cell lysate of fatty acid pre-treated cells (50 µM, 5 days) compared to the concentration detected in vehicle only treated cells. Cells were incubated with 200 µM (-)-epicatechin for 2 h. * = $p \leq 0.05$; n = 6.

FIGURE 2, Impact of DHA pre-treatment on (-)-epicatechin metabolism by Caco-2/HT29-MTX co-cultures. Cells were seeded onto permeable supports at a ratio of Caco-2/HT29-MTX 76/24 and supplemented with 50 µM DHA or vehicle for their entire differentiation time of 21 days. For metabolism experiments, cells were incubated with 200 µM epicatechin in HBSS + 1.8 mM Ca^{2+} from either the apical (a → b) or basolateral (b → a) side. After 90 min incubation, samples were taken from the apical and basolateral wells, cells were washed three times and then lysed with 80% methanol. Data represent the entire amount of a specific metabolite in that compartment. * = ≤ 0.05; n = 6.

FIGURE 3, Impact of Caco-2/HT29-MTX seeding ratio. (A) Representative widefield microscopy image of Caco-2/HT29-MTX co-culture seeded at a ratio of 76/24 at day 21 after seeding, with typical pattern of cell type distribution. Areas labelled 1 contain Caco-2 cells, areas labelled 2 contain HT29-MTX cells. (B) HT29-MTX cells are the main source of UGT activity in co-cultures. Cells were seeded on solid supports with increasing percentage of HT29-MTX cells (25, 50, 75 and 100%) and treated with either 50 µM DHA or vehicle for 21 days. Cell layers were incubated with 200 µM epicatechin from the apical side for 90 min. Glucuronic acid conjugates in supernatant and cell lysates were analyzed by LC-MS/MS. Amount of the most abundant metabolite (E-3´-glc) are shown. * = $p \leq 0.05$; n = 3.

FIGURE 4, In vitro glucuronidation of epicatechin by recombinant human UGT isoforms expressed in insect microsomes. Microsomes corresponding to 0.5 mg/mL protein were incubated with 50 µM epicatechin for 60 min at 37°C in the presence of 0.025 mg/mL alamethicin, 100 µM ascorbic acid and 1 mM UDPGA in phosphate buffer. Conjugates were analyzed by LC-MS/MS. n = 2.

FIGURE 5, UGT expression in Caco-2, HT29-MTX and HepG2 cells. (A) Expression of UGT1A1, UGT1A8 and UGT1A9 normalised to levels of the housekeeping gene GAPDH (presented as $2^{-\Delta C_T}$). (B) Impact of chronic DHA supplementation (50 µM; 21 days for Caco-2 and HT29-MTX; 5 days for HepG2) on UGT expression. * = $p \leq 0.05$; n = 5.

FIGURE 6, Specificity of antibodies used for UGT1A detection (A) and α-actinin (B). (C) Pherogram view of different amounts of whole cell lysate analyzed for standard curve construction.

FIGURE 7, Effect of chronic DHA supplementation on UGT1A protein levels in HT29-MTX cells detected with the ProteinSimple WES system. (A) Standard curve of multiplexed UGT1A and α-actinin in whole cell lysate. (B) Peak areas of UGT1A protein levels detected in whole lysate of cells treated with 50 μM DHA or vehicle for 21 days. ($t_{(6.3)}$= -4.6, p=0.003, n = 6). Error bars represent standard deviation; 400 ng of total protein was loaded per lane. (C) Reconstructed gel image view of three representative biological replicates for control and DHA treated samples. NS denotes non-specific interactions of the UGT1A antibody with the fluorescence standards used in the ProteinSimple WES system (Supplementary information).

FIGURE 8, Indirect immunofluorescence staining of UGT1A and MRP1 in HT29-MTX cells grown on permeable supports. Images were taken at 2 μm intervals along the z-axis. Rows A to D show representative images of 24 independent experiments. Staining revealed pronounced UGT1A signal in the lateral and basal plasma membrane, very similar to the plasma membrane protein MRP1. Row E shows control cell monolayers incubated with DAPI and secondary antibody only. Row F shows differential staining for UGT1A and ER marker calnexin obtained as a sum of Z-slices through the cell.

FIGURE 9, Cell surface biotinylation of HT29-MTX cells. (A) Specificity of antibodies used for UGT1A and control protein detection with the ProteinSimple SIMON system. (B) Relative peak area of protein levels detected in surface biotinylation samples after streptavidin pull down (UGT1A, Na^+/K^+-ATPase) and in whole cell lysate (GAPDH).

FIGURE 10, Impact of extracellular UDPGA on EC-3´-glc formation by HT29-MTX cells. Cells grown on solid supports were incubated with 200 μM epicatechin and 200 μM UDPGA in HBSS + 1.8 mM Ca^{2+} for 10, 30 and 60 min. Controls were incubated with epicatechin only (n = 3).

FIGURE 11, Model showing proposed UGT1A8 and UGT1A9 localization in hepatocytes and intestinal mucus cells.

Table 1. mRNA expression of UGT1A isoforms expressed in HT29-MTX cells

TaqMan primer ID		copies/ ng of cDNA (n=9)
UGT1A1	Hs02511055_s1	0.6 ± 0.2
UGT1A3	Hs04194492_g1	0.4 ± 0.2
UGT1A6	Hs01592477_m1	4.7± 1.2
UGT1A7	Hs02517015_s1	0.5 ± 0.2
UGT1A8	Hs01592482_m1	47.5 ± 10.2
UGT1A9	Hs02516855_sH	0.6 ± 0.2
UGT1A10	Hs02516990_s1	45 ± 8.9

Exact copy number of each UGT1A isoform was quantified by droplet digital PCR in triplicate of 9 biological replicates from 3 independent experiments (n=27) with TaqMan probes after DNase treatment of the mRNA.

FIGURE 1

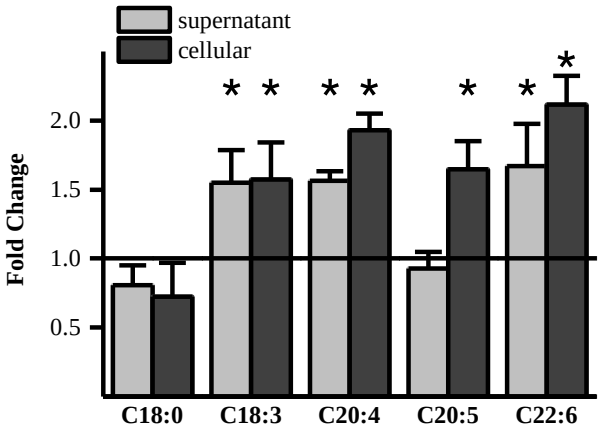
supernatant
cellular
Fold Change
2.0
1.5
1.0
0.5
C18:0
C18:3
C20:4
C20:5
C22:6

FIGURE 2

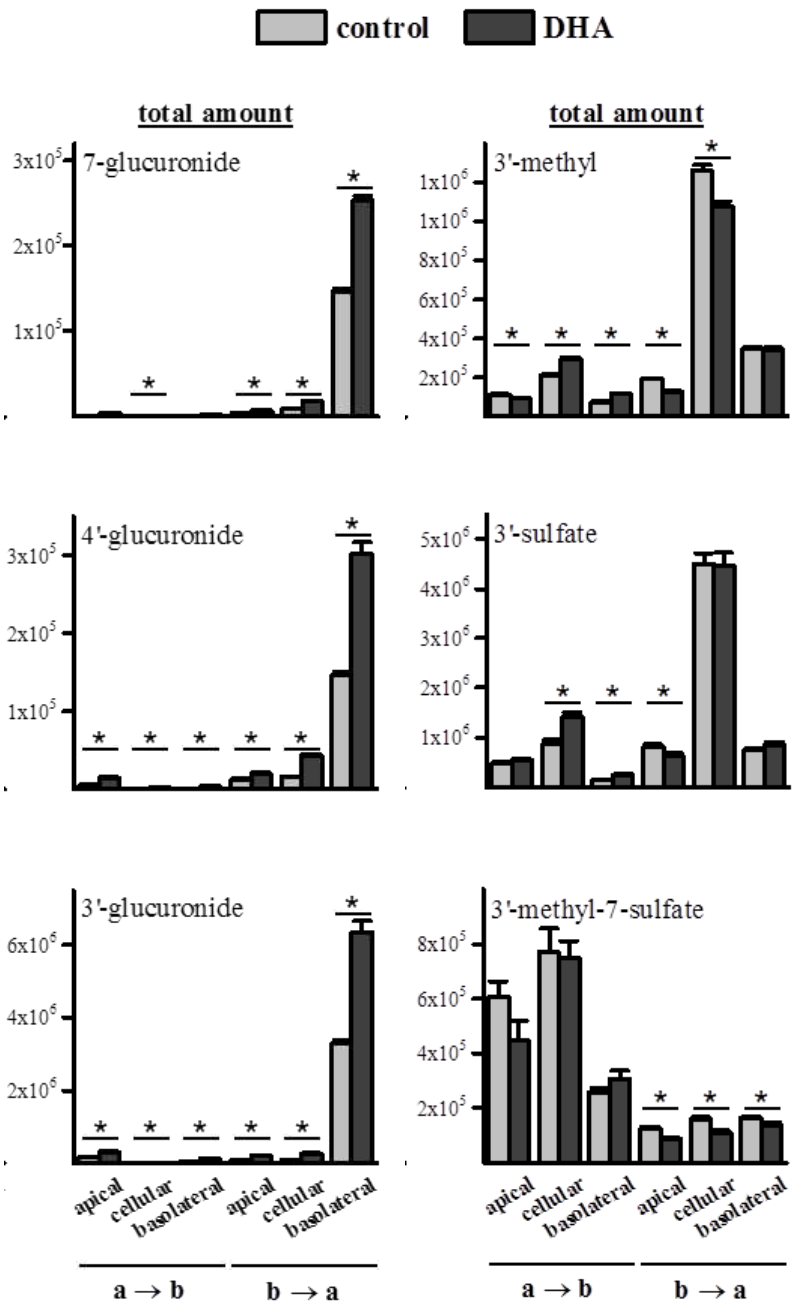
control
DHA
total amount
total amount
7-glucuronide
3'-methyl
4'-glucuronide
3'-sulfate
3'-glucuronide
3'-methyl-7-sulfate
apical
cellular
basolateral
apical
cellular
basolateral
a → b
b → a
apical
cellular
basolateral
apical
cellular
basolateral
a → b
b → a

FIGURE 3

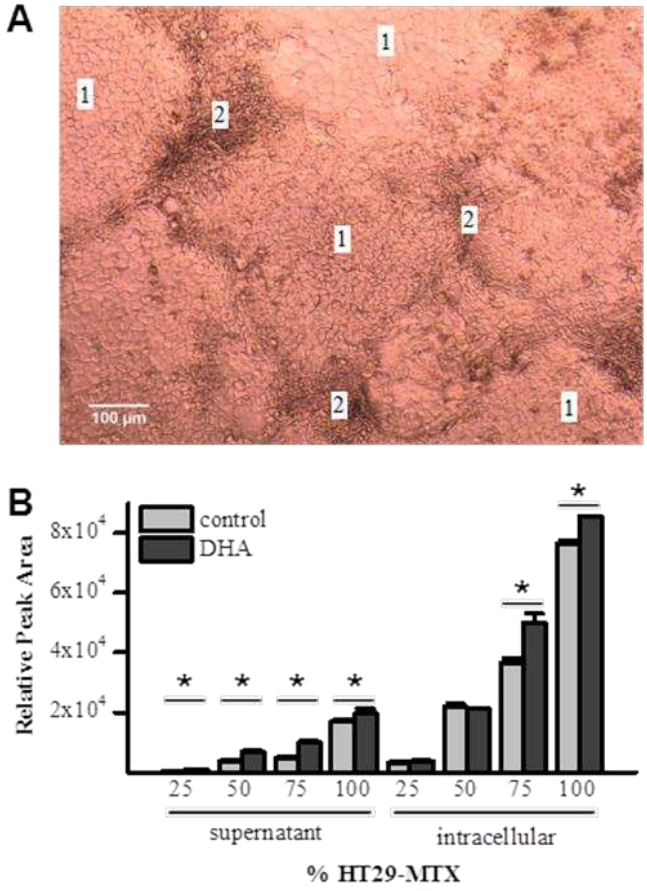
A
1
2
100 µm
B
control
DHA
Relative Peak Area
8x10^4
6x10^4
4x10^4
2x10^4
*
25
50
75
100
supernatant
intracellular
% HT29-MTX

FIGURE 4

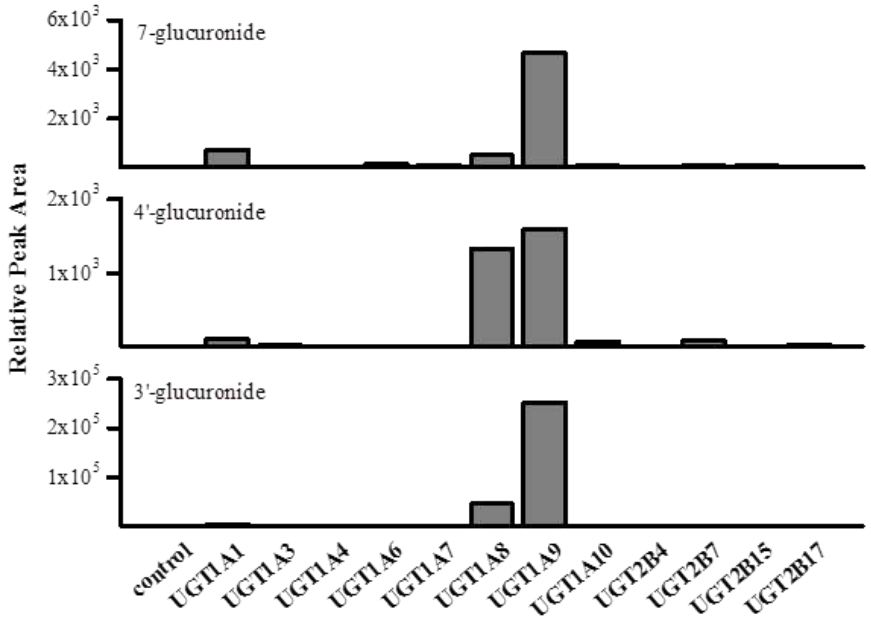
Relative Peak Area
7-glucuronide
4'-glucuronide
3'-glucuronide
6x10^3
4x10^3
2x10^3
2x10^3
1x10^3
3x10^5
2x10^5
1x10^5
control
UGT1A1
UGT1A3
UGT1A4
UGT1A6
UGT1A7
UGT1A8
UGT1A9
UGT1A10
UGT2B4
UGT2B7
UGT2B15
UGT2B17

FIGURE 5

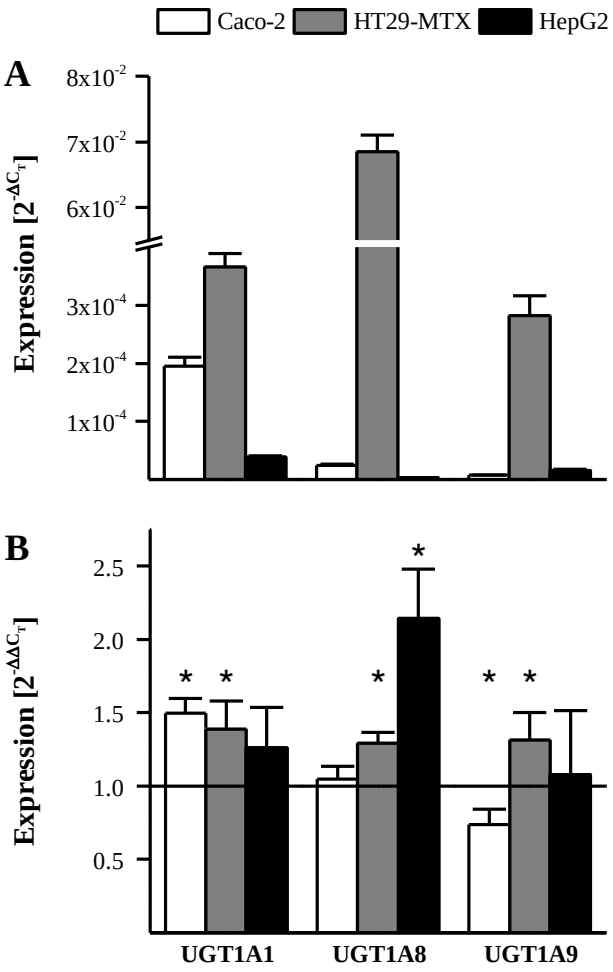
Caco-2
HT29-MTX
HepG2
A
Expression [2^-ΔC_T]
8x10^-2
7x10^-2
6x10^-2
3x10^-4
2x10^-4
1x10^-4
B
Expression [2^-ΔΔC_T]
2.5
2.0
1.5
1.0
0.5
*
UGT1A1
UGT1A8
UGT1A9

FIGURE 6

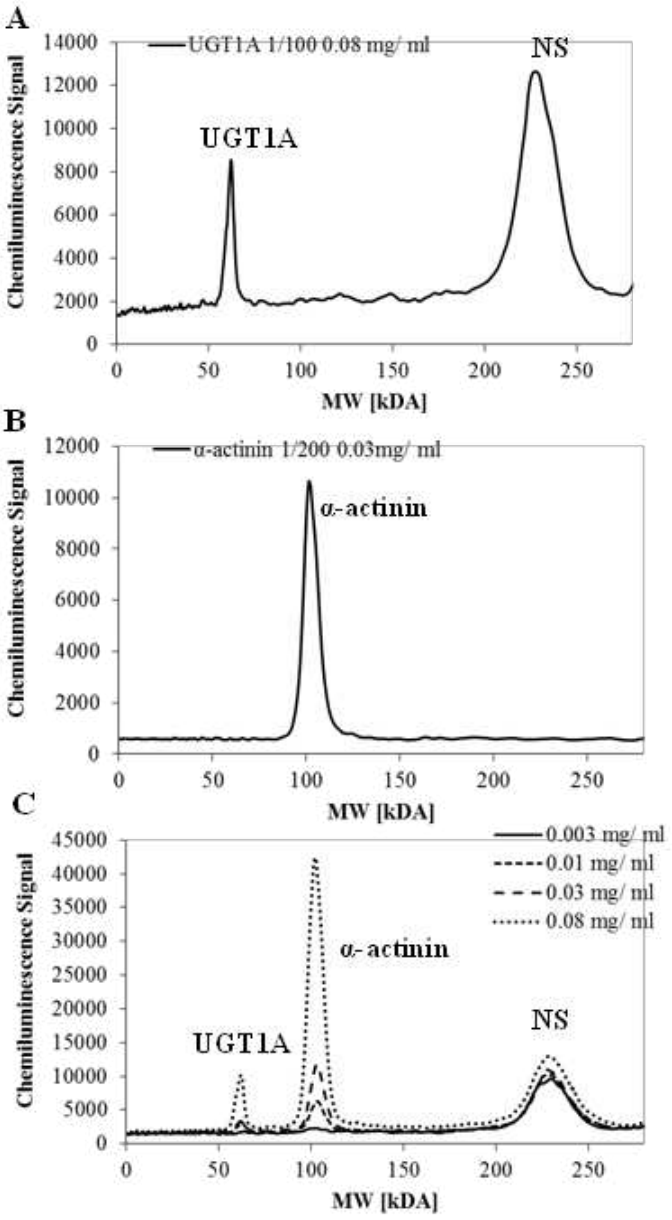
A
UGT1A 1/100 0.08 mg/ ml
NS
UGT1A
Chemiluminescence Signal
MW [kDA]
B
α-actinin 1/200 0.03mg/ ml
α-actinin
Chemiluminescence Signal
MW [kDA]
C
0.003 mg/ ml
0.01 mg/ ml
0.03 mg/ ml
0.08 mg/ ml
α-actinin
NS
UGT1A
Chemiluminescence Signal
MW [kDA]

FIGURE 7

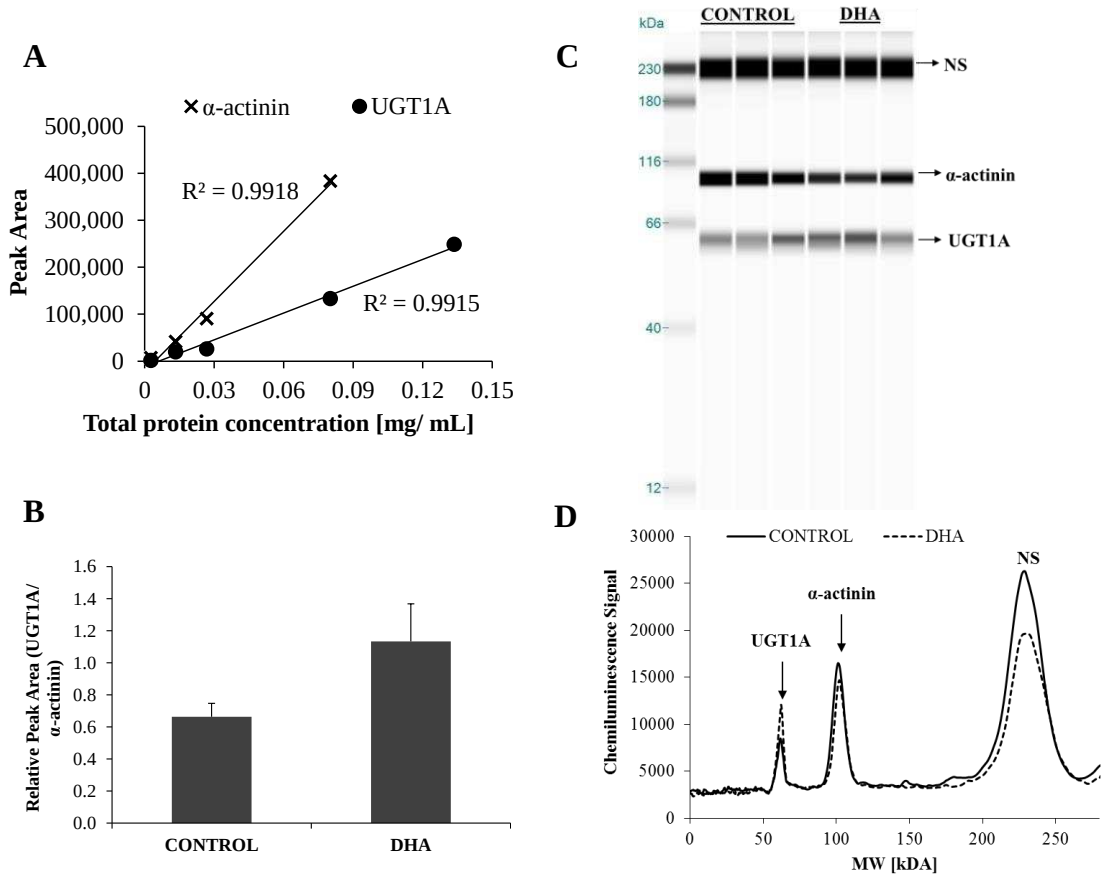
A
α-actinin
UGT1A
500,000
400,000
300,000
200,000
100,000
0
Peak Area
R² = 0.9918
R² = 0.9915
0
0.03
0.06
0.09
0.12
0.15
Total protein concentration [mg/ mL]
B
Relative Peak Area (UGT1A/ α-actinin)
1.6
1.4
1.2
1.0
0.8
0.6
0.4
0.2
0.0
CONTROL
DHA
C
kDa
CONTROL
DHA
230
180
116
66
40
12
NS
α-actinin
UGT1A
D
CONTROL
DHA
30000
25000
20000
15000
10000
5000
0
Chemiluminescence Signal
NS
α-actinin
UGT1A
0
50
100
150
200
250
MW [kDA]

FIGURE 8

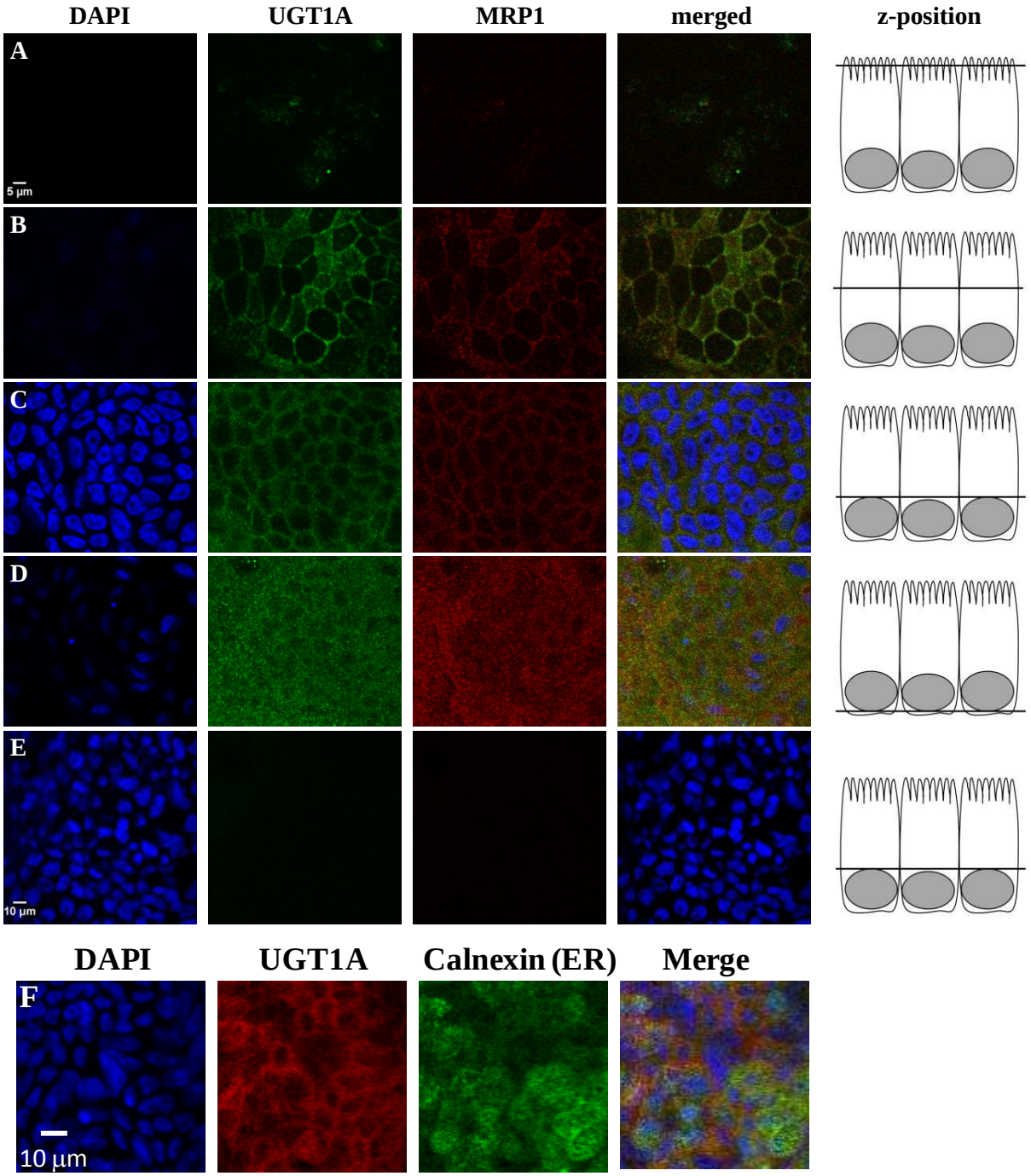
DAPI
UGT1A
MRP1
merged
z-position
A
5 µm
B
C
D
E
10 µm
DAPI
UGT1A
Calnexin (ER)
Merge
F
10 µm

FIGURE 9

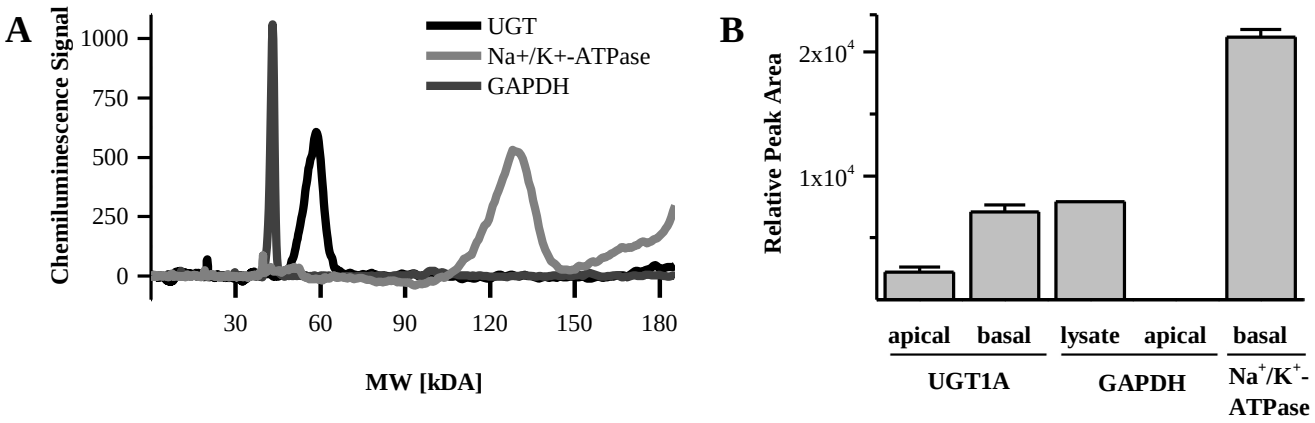
A
Chemiluminescence Signal
1000
750
500
250
0
30
60
90
120
150
180
MW [kDA]
UGT
Na+/K+-ATPase
GAPDH
B
Relative Peak Area
2x10^4
1x10^4
apical
basal
lysate
apical
basal
UGT1A
GAPDH
Na+/K+-ATPase

FIGURE 10

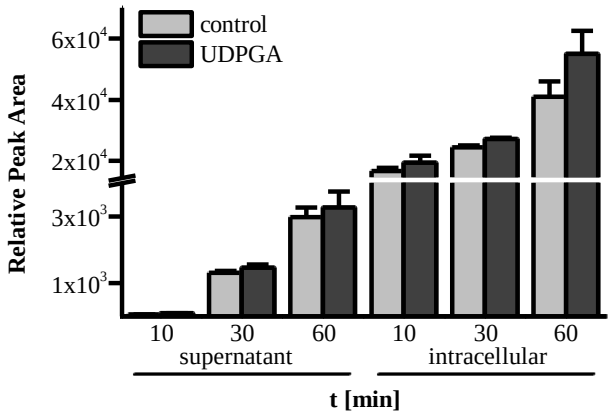
control
UDPGA
Relative Peak Area
6x10^4
4x10^4
2x10^4
3x10^3
1x10^3
10
30
60
10
30
60
supernatant
intracellular
t [min]

FIGURE 11

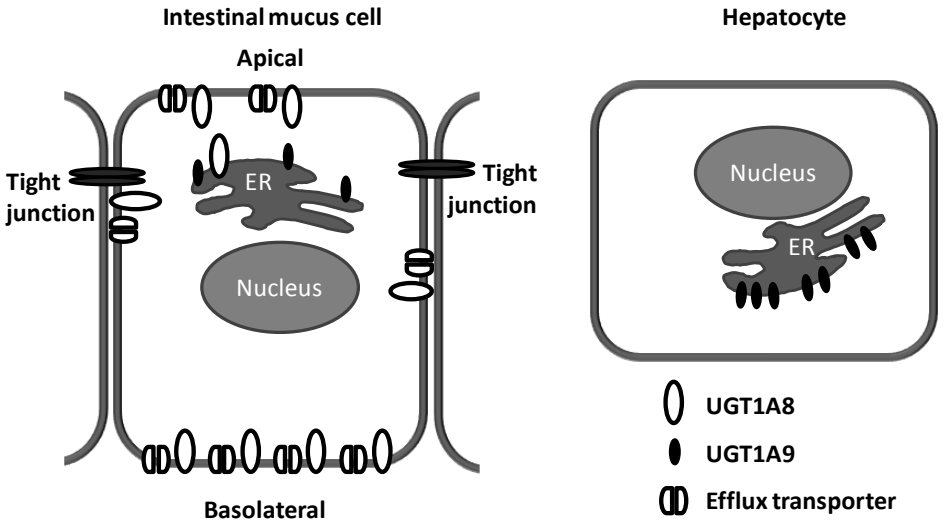
Intestinal mucus cell
Apical
Tight junction
ER
Tight junction
Nucleus
Basolateral
Hepatocyte
Nucleus
ER
UGT1A8
UGT1A9
Efflux transporter